

This is the peer reviewed version of the following article: H. Xia, Y. Zhang, W. Deng, K. Liu, X. Xia, C.-J. Su, U.-S. Jeng, M. Zhang, J. Huang, J. Huang, C. Yan, W.-Y. Wong, X. Lu, W. Zhu, G. Li, Novel Oligomer Enables Green Solvent Processed 17.5% Ternary Organic Solar Cells: Synergistic Energy Loss Reduction and Morphology Fine-Tuning. *Adv. Mater.* 2022, 34, 2107659, which has been published in final form at <https://doi.org/10.1002/adma.202107659>. This article may be used for non-commercial purposes in accordance with Wiley Terms and Conditions for Use of Self-Archived Versions. This article may not be enhanced, enriched or otherwise transformed into a derivative work, without express permission from Wiley or by statutory rights under applicable legislation. Copyright notices must not be removed, obscured or modified. The article must be linked to Wiley's version of record on Wiley Online Library and any embedding, framing or otherwise making available the article or pages thereof by third parties from platforms, services and websites other than Wiley Online Library must be prohibited.

Novel Oligomer Enables Green Solvent Processed 17.5% Ternary Organic Solar Cells: Synergistic Energy Loss Reduction and Morphology Fine-tuning

Hao Xia, Ying Zhang, Wanyuan Deng, Kuan Liu, Xinxin Xia, Chun-Jen Su, U-Ser

Jeng, Miao Zhang, Jiaming Huang, Jingwei Huang, Cenqi Yan, Wai-Yeung Wong,

Xinhui Lu, Weiguo Zhu,* Gang Li*

H. Xia, J. Huang (Jingwei Huang), Prof. W. Zhu
School of Materials Science and Engineering, Jiangsu Engineering Laboratory of Light-Electricity-Heat Energy-Converting Materials and Applications Jiangsu Collaborative Innovation Center of Photovoltaic Science and Engineering National Experimental Demonstration Center for Materials Science and Engineering,
Changzhou University,
Changzhou 213164, China
E-mail: zhuwg18@126.com

H. Xia, Y. Zhang, Dr. K. Liu, J. Huang (Jiaming Huang), Dr. C. Yan, Prof. G. Li
Department of Electronic and Information Engineering, Research Institute for Smart Energy (RISE), The Hong Kong Polytechnic University,
Hung Hum Kowloon, Hong Kong 999077, China
E-mail: gang.w.li@polyu.edu.hk

Dr. W. Deng
State Key Laboratory of Luminescent Materials and Devices, Institute of Polymer Optoelectronic Materials and Devices,
South China University of Technology,
Guangzhou 510640, China

X. Xia, Prof. X. Lu
Department of Physics,
The Chinese University of Hong Kong,
New Territories, Hong Kong 999077, China

Dr. C.-J. Su, Dr. U.-S. Jeng
National Synchrotron Radiation Research Center,
Hsinchu Science Park, Hsinchu 30076, Taiwan

Dr. M. Zhang, Prof. W.-Y. Wong
Department of Applied Biology and Chemical Technology,
The Hong Kong Polytechnic University,
Hung Hum Kowloon, Hong Kong 999077, China

Abstract:

The large non-radiative recombination is the main factor that limits state-of-the-art organic solar cells (OSCs). In this work, we synthesized two novel structurally similar oligomers (5BDTBDD and 5BDDBDT) with D-A-D-A-D and A-D-A-D-A configuration for high-performance ternary OSCs with low energy loss. As third components, these PM6 analogue oligomers effectively suppress the non-radiative recombination of the ternary OSCs. Although the HOMO energy levels of 5BDTBDD and 5BDDBDT are higher than that of PM6, the oligomers showed ultra-high EQE_{EL} of 0.05% and improved V_{OC} was achieved in ternary OSCs, indicating that suppressing non-radiative recombination overweighs the common belief of deeper HOMO requirement in third component selection. Moreover, the different compatibility of 5BDTBDD and 5BDDBDT with PM6 and BTP-BO4Cl fine-tunes the morphology of the active layer and forms synergistic effects. The ternary devices based on PM6:5BDTBDD:BTP-BO4Cl and PM6:5BDDBDT:BTP-BO4Cl achieve a significantly improved PCEs of 17.54% and 17.32%, representing the state-of-the-art OSCs processed by green solvent of *o*-xylene. The strategy using novel oligomer as third component also has very wide composition tolerance. This is the first work that demonstrates novel structurally compatible D-A type oligomers are effective third components, and provides new understanding of energy loss mechanisms towards high performance OSCs.

KEYWORDS: oligomers, ternary organic solar cells, low energy loss, green solvent, wide composition tolerance.

1. Introduction

Organic solar cells (OSCs) have attracted abroad attention and extensive research interest due to their distinct advantages of light weight, flexibility, semitransparency and low cost.^[1-4] Recently, the performance of OSCs has been improved rapidly owing to the great efforts on innovative materials and device structures, especially the fused-ring non-fullerene acceptors (NFAs).^[5-13] Thanks to the advantages of easily modified structures, tunable energy levels, strong and wide absorption in the near infrared (NIR) region,^[5] the single-junction devices of polymer organic solar cells (PSCs) have achieved the power conversion efficiencies (PCEs) over 18%.^[6-10] Nevertheless, compared with silicon and perovskite solar cells, the larger energy loss (E_{loss}) is a key issue to restrict the further performance improvement of OSCs.^[14] Here, the E_{loss} is defined as $E_g - qV_{\text{OC}}$, in which E_g is the optical band gap of the active layer, V_{OC} is the open circuit voltage of the cells, and q is the elementary charge. It is positively correlated to the difference between the highest occupied molecular orbital (HOMO) level of the donor and the lowest unoccupied molecular orbital (LUMO) level of the acceptor. Generally, to solve this issue, one strategy is to develop a low energy loss binary system,^[14,15] another is to incorporate the third component with deeper HOMO level donors^[16,17] or shallower LUMO level acceptors into binary host matrix to regulate the energy level of the active layer and construct low energy loss ternary system.^[18,19]

The restricted absorption range and morphological optimization of OSCs also remain challenging for OSCs. Multiple-component, in particular ternary strategy has become an effective way to solve the issues above. In general, the efficient ternary OSCs consisting of one donor and two acceptors (D:A₁:A₂) or two donors and one acceptor (D₁:D₂:A) are constructed by rationally selecting the third component under the following considerations: complementary absorption ranges,^[19,20] aligned energy levels,^[21-23] alloy^[19,21] or parallel,^[22] compatibility^[24-26] and/or crystalline properties,^[27,28] which are effective to optimize the key photovoltaic parameters: V_{OC} , short-circuit current density (J_{SC}), and fill factor (FF). However, the morphology of

ternary blend films becomes more complicated due to multi-component interactions. As we know, the PM6:Y-series are the most reported binary systems. In order to further extend absorption range and improve morphology of active layers, ternary OSCs were structured using several strategies on the basis of the PM6:Y-series host matrixes. (1) Fullerene acceptors: Hou et al added the fullerene acceptor PC₇₁BM into the classical binary PM6:Y6 host matrix, which improved the V_{OC} from 0.834 to 0.845 V, J_{SC} from 24.8 to 25.4 mA cm⁻² and FF from 0.741 to 0.770.^[24] (2) Non-fullerene fused-ring small-molecular acceptors (SMAs): Yan et al constructed ternary OSCs using dual non-fullerene acceptors BTP-Ph:BTP-Th, which promoted J_{SC} from 24.7 to 25.2 mA cm⁻² and FF from 0.762 to 0.786.^[13] (3) Polymer donor: Zhang et al adopted polymer donor S3 into binary PM6:Y6 host matrix, which raised the three key parameters synchronously: V_{OC} from 0.844 to 0.856 V, J_{SC} from 25.13 to 25.86 mA cm⁻² and FF from 0.756 to 0.792.^[17] However, there are very few research using small molecular donors to optimize PM6:Y6-based binary OSCs. Here, the special materials produced by small molecularization of polymers with multiple electron donor and acceptor (D-A) repetitive units, so-called D-A type oligomers, were demonstrated to be the superior third component candidates.^[29-33] D-A oligomers integrate the merits of polymer and small molecule: well-defined molecular structure, less batch-to-batch variations and good film formation.

In this work, an A-D-A-D-A type oligomer of 5BDDBDT was further designed and synthesized on the base of the D-A-D-A-D type oligomer of 5BDTBDD with 4,8-di(6-ethylhexylthiophen-2-yl)benzo[1,2-b:4,5-b']dithiophene (BDT) and benzo[1,2-c:4,5-c']dithiophene-4,8-dione (BDD) units in our previous work.^[33] The ternary OSCs based on the PM6:5BDTBDD:BTP-BO4Cl and PM6:5BDDBDT:BTP-BO4Cl blends were constructed, where 5BDTBDD and 5BDDBDT were used as the third components in the PM6:BTP-BO4Cl binary blend, respectively. Processed by green solvent of *o*-xylene, an excellent PCE of 17.54% with a V_{OC} of 0.843 V, a J_{SC} of 26.83 mA cm⁻² and a FF of 77.43% was achieved in the PM6:5BDTBDD:BTP-BO4Cl ternary OSCs, while a high PCE of 17.32% with a V_{OC} of 0.839 V, a J_{SC} of 26.68 mA cm⁻² and a FF of 77.42% was obtained in the PM6:5BDDBDT:BTP-BO4Cl ternary OSCs. The promotion of J_{SC}

could be attributed to the larger electrostatic potential between 5BDTBDD or 5BDDBDT with the acceptor, which promotes the dissociation of the excitons. The fine-tuned active layer morphology and the improved carrier mobility contribute to the better FFs in the optimized ternary OSCs. More importantly, the V_{OC} of ternary devices was surprisingly improved, although the HOMO energy levels of the oligomers 5BDTBDD and 5BDDBDT are higher than that of PM6, which is attributed to the decreased E_{loss} , especially non-radiative recombination. It is noteworthy that even when incorporating 50% 5BDTBDD, a comparable 16.15% PCE was obtained in ternary devices, indicating the high tolerance of ternary blends to the proportion of the third component. Overall, our work provides a new, feasible and effective strategy to pave the way towards highly efficient OSCs by employing oligomers as the third components.

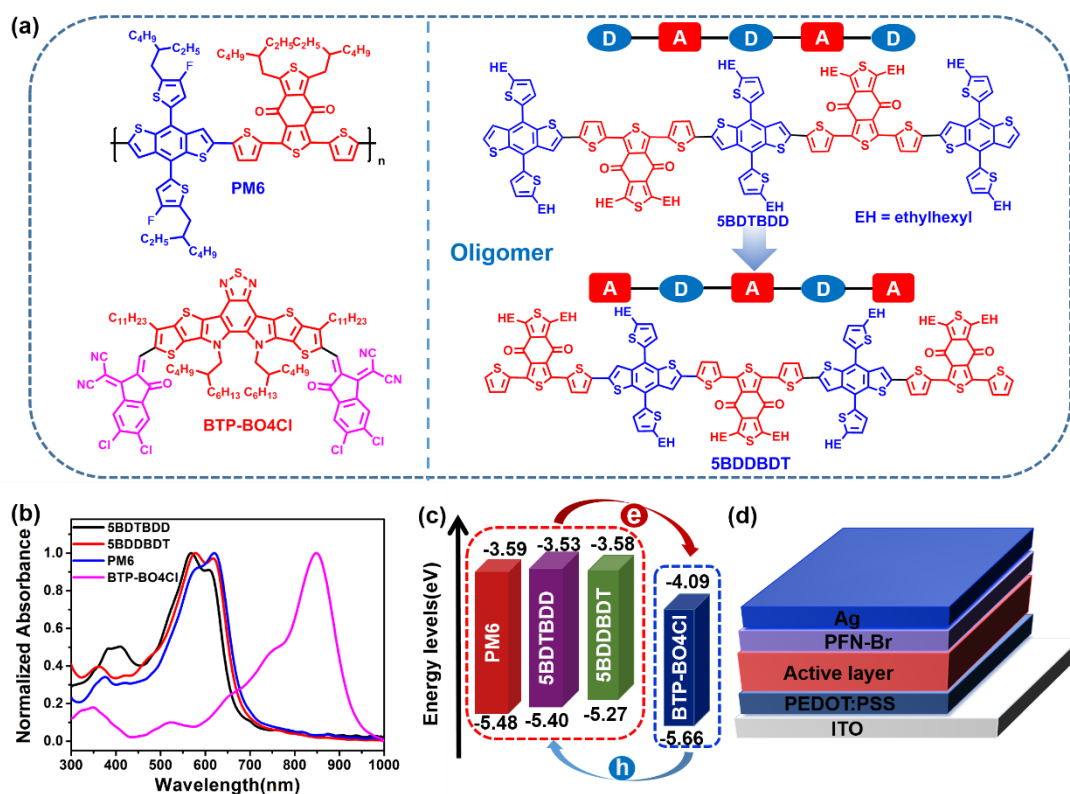


Figure 1. a) Chemical structures of PM6, BTP-BO4Cl, 5BDTBDD and 5BDDBDT. b) Normalized UV-vis absorption spectra in neat films. c) Energy levels of PM6, 5BDTBDD, 5BDDBDT and BTP-BO4Cl. d) Schematic diagram of conventional device structure.

2. Results and Discussion

Synthesis, Thermal, Optical and Electrochemical Properties

The synthetic routes of 5BDTBDD are shown in our previous work,^[33] and that of 5BDDBDT are depicted in **Scheme 1** of Electronic Supporting Information (ESI). 1,3-Dibromo-5,7-bis(2-ethylhexyl)benzo[1,2-c:4,5-c']dithiophene-4,8-dione (compound **1**) was reacted with 2-(tributylstannyl)thiophene to form compound **2** in a yield of 93% by Stille coupling. Compound **4** was synthesized by a reaction between 4,8-bis(5-(2-ethylhexyl)thiophen-2-yl)benzo[1,2-b:4,5-b']dithiophene (compound **3**) and carbon tetrabromide in a yield of 86% under low temperature and n-BuLi. By controlling the ratio of reactants, compounds **5** and **6** were synthesized between compound **4** and trimethyltin chloride in high yields, respectively, under the effect of n-BuLi. Compound **7** was provided by a unilateral coupling of compounds **4** and **5** with a yield of 48%. 5BDDBDT was obtained by a Stille coupling between **6** and **7** in a yield of 55%. All synthetic details are provided in ESI. The resulting oligomer 5BDDBDT was fully characterized by ¹H, ¹³C NMR. In addition, the oligomer 5BDDBDT was characterized by MALDITOF-MS. The oligomer 5BDTBDD and 5BDDBDT show good solubility in common solvents, such as dichloromethane, chloroform and chlorobenzene.

The thermogravimetry curves of 5BDTBDD and 5BDDBDT are depicted in Figure S1a. Under a nitrogen atmosphere, the decomposition temperatures over 410 °C at 5% weight loss are observed for both molecules, indicating their good thermal stability. Differential scanning calorimetry (DSC) plots of 5BDTBDD and 5BDDBDT are shown in Figure S1b. The feeble melting temperature (T_m) and crystallization peak (T_c) is observed for the 5BDTBDD oligomer upon second heating and first cooling. In contrast, there is no significant melting and crystallization peak observed in 5BDDBDT, indicating the abated crystallization of oligomer 5BDDBDT.

The optical properties of donors 5BDTBDD, 5BDDBDT, PM6 and acceptor BTP-BO4Cl were investigated by ultraviolet–visible (UV–vis) absorption spectra in dilute chloroform solution (10^{-5} mol L⁻¹) (Figure S2a) and thin films (**Figure 1b**, Figure S2b). Figure S2c shows the absorption spectra of blend films with different component proportions. The relevant optical data are listed in **Table 1**. As shown in Figure S2a and S2b, the maximum extinction coefficients of 5BDTBDD and 5BDDBDT are 1.35×10^5

and $1.38 \times 10^5 \text{ M}^{-1} \text{ cm}^{-1}$ in chloroform solution, respectively. The absorption coefficients of 5BDTBDD, 5BDDBDT and PM6 in neat films are 7.22×10^4 , 8.37×10^4 and $1.24 \times 10^5 \text{ cm}^{-1}$, respectively. In addition, from solution to thin film, both molecules exhibit a prominently red-shifted absorption spectrum due to their tighter intermolecular stacking in the thin films.^[34] Moreover, the absorption spectra of 5BDTBDD and 5BDDBDT are similar to that of PM6, but slightly blue-shifted. It is found that three donor molecules here exhibit a complementary absorption spectrum with the acceptor BTP-BO4Cl in the whole region from 300 to 1000 nm, which is beneficial for photon harvesting. The optical band gaps (E_g^{opt}) of 5BDTBDD, 5BDDBDT and PM6 in film state are calculated to be 1.86, 1.83 and 1.81 eV, respectively.

The electrochemical potentials of pure donor and acceptor, and mixtures with different proportions of oligomer and PM6 were measured using cyclic voltammetry (CV) method (Figure S3), and the detailed data are shown in **Table 1**. The HOMO and LUMO levels of 5BDTBDD, 5BDDBDT and PM6 are calculated from the onset oxidation potential and reduction potential as -5.40, -5.27, -5.48, and -3.59, -3.53, -3.58 eV, respectively by empirical equation.^[35] Obviously, when compared with PM6, oligomers of 5BDTBDD and 5BDDBDT exhibit significantly elevated HOMO energy levels due to their lack of F atoms. Thus, cascade energy level alignments of ternary blends are constructed for both systems of 5BDTBDD/PM6/BTP-BO4Cl and 5BDDBDT/PM6/BTP-BO4Cl, as shown in **Figure 1**. The oligomeric components are likely to provide an additional charge transfer pathway between the host donor and acceptor.^[36,37] Figure S3 and Table S1 show the energy levels of the mixed donors with different oligomer proportions. It was found that the HOMO energy levels vary linearly for the oligomer:PM6 blend films with different proportions of oligomer. In addition, all donors of 5BDTBDD, 5BDDBDT and PM6 show appropriate HOMO and LUMO energy levels to the acceptor BTP-BO4Cl, which ensures enough force to promote exciton dissociation.^[38,39]

Table 1. Optical and electrical properties of 5BDTBDD, 5BDDBDT and PM6.

Donor	λ_{\max} (nm)		$\lambda_{\text{onset, film}}$ (nm)	E_g^{opt} (eV) ^a	E_{HOMO} (eV) ^b	E_{LUMO} (eV) ^b
	Solution	Film				
5BDTBDD	512	568, 609	665	1.86	-5.40	-3.53
5BDDBDT	518	577, 618	678	1.83	-5.27	-3.58
PM6	550	580, 620	684	1.81	-5.48	-3.59

^aCalculated from the absorption band edge of the films, $E_g^{\text{opt}} = 1240/\lambda_{\text{onset}}$ ^bCalculated from empirical equation: $E_{\text{HOMO/LUMO}} = -(E_{\text{ox/red}} + 4.8)$ eV (The formal potential of Fc/Fc⁺ is 0.43 V vs. Ag/AgCl measured in this work)

Theoretical Calculations

The density functional theory (DFT) at the B3LYP/6-31G* basis set using Gaussian 09W program [40] was adopted to further investigate the configuration, energy levels and electrostatic potential (ESP) of monomers (BDT, BDT-F, BDD), oligomers (5BDTBDD, 5BDDBDT), PM6 fragments, and BTP-BO4Cl, as shown in **Figure 2** and Figure S4. All long alkyl side chains in molecules are truncated to shorter methyl groups to simplify calculations. The optimal molecular configuration, HOMO, LUMO energy levels and their electron cloud distribution of 5BDTBDD, 5BDDBDT and PM6 fragments are shown in Figure S4. As a result, all of them present good molecular planarity, especially PM6, which is conducive to intermolecular π - π stacking, that is consistent with the UV-vis test results. Besides, PM6 and 5BDDBDT show the deepest and shallowest HOMO levels, respectively, which is consistent with the result of CV test. According to the ESP result, the difference between 5BDTBDD or 5BDDBDT with PM6 fragments is the fluorination of the BDT monomer, which has a significant influence on the distribution of ESP in the BDT units as introducing fluorine atom. As is shown in the ESP maps of BDT and BDT-F, the ESP values increased significantly on most of the BDT-F surface in comparison with BDT, which could be due to the strong electron-drawing ability of F atom. To make the distribution of ESP values of 5BDTBDD, 5BDDBDT, PM6 and BTP-BO4Cl more clearly visualized, the ESP surface area distributions of the molecules with different ESP are shown in **Figure 2**. It is observed that 5BDTBDD and 5BDDBDT exhibit lower ESP surface area, indicating lower ESP values of two oligomers than that of PM6 fragments. Most of the conjugated main chains of BTP-BO4Cl possess positive ESP due to the strong electron withdrawing ability of the end groups. It has been reported that a larger difference of ESP between donor and acceptor can induce larger intermolecular electric field (IEF), which is more favorable for the exciton dissociation.^[41]

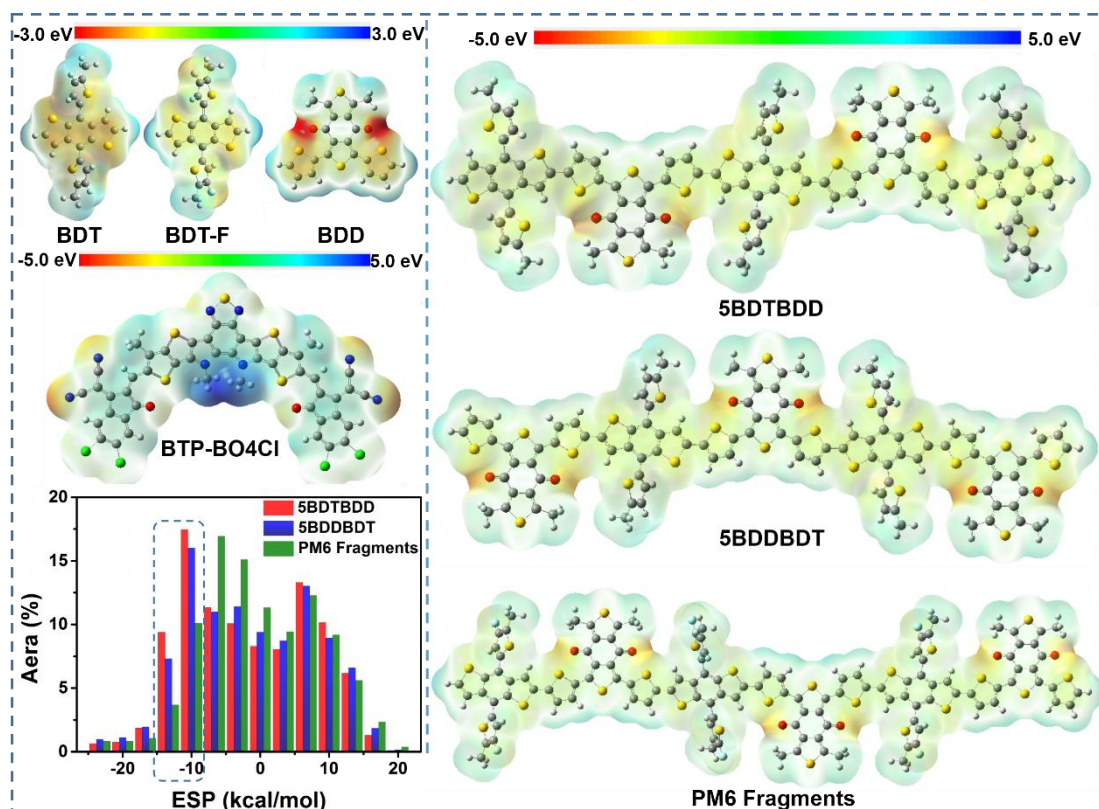


Figure 2. ESP map of BDT, BDT-F, BDD, BTP-BO4Cl, 5BDTBDD, 5BDDBDT and PM6 fragments.

Photovoltaic Properties

We incorporated oligomer 5BDTBDD as a third component into a high-efficiency system of PM6:BTP-BO4Cl to fabricate ternary OSCs with a conventional device structure of Glass/ITO/ PEDOT:PSS/Active layer/PFN-Br/Ag, as shown in **Figure 1d**. All binary and ternary OSCs were fabricated by maintaining the total D/A weight ratio as 1:1.2 with various contents of 5BDTBDD (0%, 10%, 30%, 50% and 100% by weight) using a halogen-free solvent *o*-xylene. More details of devices fabrication are described in the ESI. The typical current density–voltage (J – V) curves of these OSCs are depicted in **Figure 3a**, and the corresponding device parameters are summarized in **Table 2**. The binary OSCs based on PM6:BTP-BO4Cl obtained a PCE of 16.13%, with a V_{OC} of 0.831 V, a J_{SC} of 25.97 mA cm⁻² and a FF of 74.69%, which is consistent with the related reported results.^[42] When the PM6:5BDTBDD:BTP-BO4Cl ratio is 0.9:0.1:1.2, the optimized device delivered the highest PCE of 17.54%, and the corresponding V_{OC} , J_{SC} and FF are 0.843 V, 26.83 mA cm⁻² and 77.43%, respectively. The enhanced J_{SC} in optimized 10% device may be linked to the larger ESP difference

between 5BDTBDD and BTP-BO4Cl as theoretically calculated above. After the addition of 5BDTBDD (30%), the J_{SC} decreased to 24.73 mA cm^{-2} , but the PCE still remains at a higher value (16.38%) than the PM6:BTP-BO4Cl binary blend. Further addition of 5BDTBDD (50%) resulted in reduction of J_{SC} s (24.66 mA cm^{-2}). The decreased J_{SC} s in ternary devices (30% and 50%) are mainly due to the weaker absorption in donors' region around 600 nm (see Figure S2c and Table S2). It is worth noting that FFs still achieve higher values of 77.23% and 75.47% in ternary devices (30% and 50%), respectively, which may result from the good compatibility of guest donor with the host components and will be discussed in the morphology part. Furthermore, with the loading of 5BDTBDD, increase of V_{OC} is obviously observed from 0.831 V for 0% device, to 0.843 V for 10% device, 0.858 V for 30% device, 0.868 V for 50% device and 0.901 V for 100% device. Although J_{SC} decreases slightly with more 5BDTBDD, the synchronous improvements of FF and V_{OC} in 50% device enable a compatible PCE of 16.15% with respect to the binary device, indicating excellent composition tolerance in ternary OSCs. Noticeably, according to the CV results, the HOMO level (-5.40 eV) of 5BDTBDD is shallower than that of PM6 (-5.48 eV), which is against the mainstream strategy of adding the third component with deeper HOMO level to increase the V_{OC} . The specific details will be analyzed below. We also fabricated additive-free devices for both binary and ternary OSCs, the detailed performances can be found in ESI (Figure S5, Table S3). The ternary devices of 10% 5BDTBDD without DIO show a better PCE of 15.65% with an enhanced V_{OC} of 0.845 V, comparable J_{SC} and FF compared to the control counterparts, implying that a small amount of 5BDTBDD seems to act as a "solid additive" to tune the morphology of active layer. Besides, to verify the universality of this strategy, we used another oligomer 5BDDBDT as the third component with similar structural fragment to PM6 in PM6:BTP-BO4Cl system and investigated the performances of ternary OSCs based on PM6:5BDDBDT:BTP-BO4Cl. Similarly, when adding 10% 5BDDBDT, an optimum PCE of 17.32% was obtained with a V_{OC} of 0.839 V, a J_{SC} of 26.68 mA cm^{-2} , and a FF of 77.42%, demonstrating the universality of this oligomeric ternary strategy.

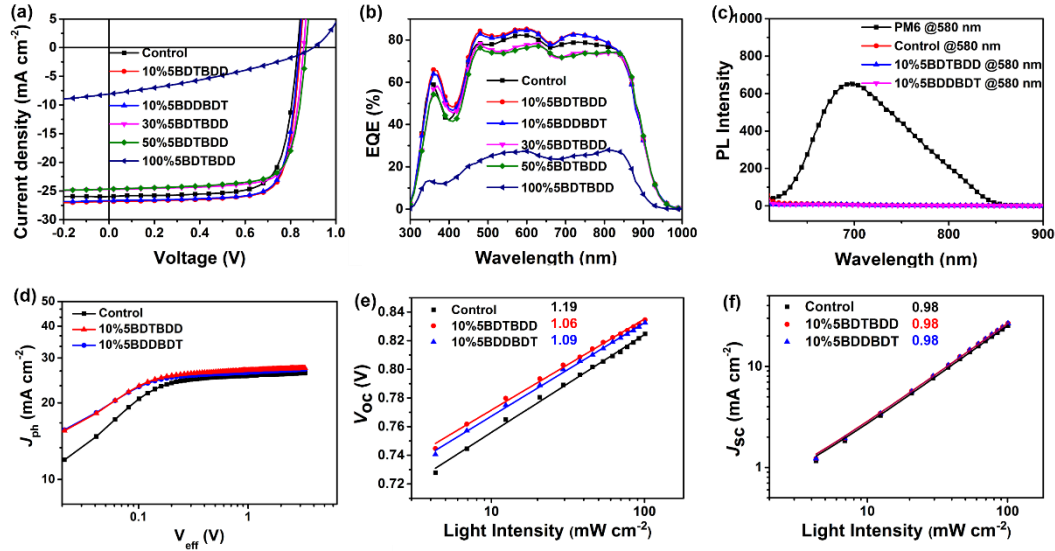


Figure 3. a) J - V curves and b) EQE curves of control and ternary devices under optimal processing condition. c) Photoluminescent spectra of the pure and blend films excited at 580 nm. d) The curves of J_{ph} versus V_{eff} in the optimized solar cells. e) The dependence of P_{light} on V_{OC} of the optimized solar cells. f) The dependence of P_{light} on J_{sc} of the optimized solar cells.

With the interesting lower abnormal V_{OC} loss in mind, we further explore the higher V_{OC} device based on 50%PM6:50%5BDTBDD:BTP-BO4Cl. The variation of V_{OC} is realized by optimizing the D:A weight ratio for both binary and ternary devices, the photovoltaic parameters are listed in Table S4. By increasing the D:A ratio from 1:1.2 to 1:0.8 in 50% device, a higher V_{OC} of 0.884 V was achieved with an inhibited E_{loss} as low as 0.506 eV, which is among the lowest values in the state-of-the-art OSCs.^[36] To further confirm the abnormal increase of V_{OC} , the parent polymer PBDB-T of both oligomers with higher HOMO energy level was chosen to construct the ternary OSCs for comparison, i.e., traditional two polymeric donors-one acceptor case. As shown in Figure S5a and Table S2, the PCE of ternary device dropped sharply to be less than 14% after adding 5% PBDB-T, and further to 12.25% with the 10% PBDB-T addition, mainly suffering from the significantly reduced V_{OC} and FF. The severe decline of V_{OC} from 0.831 V in binary device to 0.795 V for 5% device and 0.772 V for 10% device was attributed to the shallower HOMO energy level of PBDB-T.^[35] In view of the decreased FFs from 74.69% in binary to 69.70% (5%) and 59.32% (10%), we speculate that the long-chain nature of PBDB-T would be more likely to be self-aggregate to form separated domains at large scale and thus disturb the optimal phase separation in the

original binary blend.^[17] This result demonstrates the unique merits of utilizing oligomers with higher HOMO level as the third components in constructing high-performance OSCs. External quantum efficiency (EQE) spectra are presented in **Figure 3b**. The optimal ternary devices with 10% 5BDTBDD and 10% 5BDDBDT exhibited higher EQE values in both the donor and acceptor absorption ranges than the relevant binary devices. Moreover, all J_{SC} s obtained from the EQE spectral integration coincide with the values obtained from the J - V measurements under the AM 1.5G solar spectrum (within less than 4% error).

Table 2. The photovoltaic parameters of the binary and ternary devices.

Third component ratio	Thickness (nm)	V_{oc} (V)	J_{SC}^a (mA cm ⁻²)	J_{SC}^{EQE} (mA cm ⁻²)	FF (%)	PCE _{max} ^b (%)
Control ^c	120±5	0.831	25.97	25.10	74.69	16.13
10%5BDTBDD ^c	120±5	0.830±0.001	25.76±0.26	26.02	74.41±0.27	16.08±0.08
		0.843	26.83		77.43	17.54
10%5BDDBDT ^c	120±5	0.841±0.002	26.49±0.40	25.86	77.26±0.49	17.22 ±0.34
		0.839	26.68		77.42	17.32
30%5BDTBDD ^c	110±6	0.836±0.003	26.64±0.26	24.09	77.22±0.45	17.24 ±0.22
		0.858	24.73		77.23	16.38
50%5BDTBDD ^d	110±6	0.856±0.002	24.54±0.45	23.92	77.04±0.15	16.23±0.38
		0.868	24.66		75.47	16.15
100%5BDTBDD ^e	100±5	0.866±0.002	24.54±0.17	8.00	75.23±0.25	16.03±0.20
		0.901	8.10		33.26	2.43
		0.889±0.008	7.91±0.61		31.14±1.99	2.27±0.16

^a J_{SC} measured from devices; ^bPCE obtained from 20 devices, with 0.5% DIO additive; ^cD:A = 10:12 mg/mL; ^dD:A = 13:15.6 mg/mL; ^eD:A = 15:18 mg/mL.

Charge Separation, Transport and Recombination

To understand the enhancement of J_{SC} and FF in ternary OSCs, steady-state photoluminescence (PL) spectra were measured for the binary and ternary OSCs, and the results are shown in **Figure 3c**. The PM6 neat film, binary and ternary blend films were excited with 580 nm of light. An intense emission peak was observed in PM6 neat film. The emission of the PM6 neat film is almost completely quenched in the PM6:BTP-BO4Cl binary, PM6:5BDTBDD:BTP-BO4Cl and PM6:5BDDBDT:BTP-BO4Cl ternary blend films with high quenching efficiencies of 95.96%, 98.32% and 97.88%, respectively. Moreover, the emission peak of the 5BDTBDD and 5BDDBDT films is also quenched in the PM6:5BDTBDD:BTP-BO4Cl and PM6:5BDDBDT:BTP-BO4Cl ternary blend films with quenching efficiencies of 99.49% and 99.44% (Figure S6), respectively. The results show that the more efficient exciton separation in ternary blend films contributes to higher J_{SC} of ternary devices.^[43]

On the other hand, the charge transport properties of the binary and ternary blend films were investigated via the space-charge limited current (SCLC) method (Figure

S7), and relevant data are displayed in Table S5.^[44] The structures of hole-only and electron-only devices are ITO/PEDOT:PSS/Active Layer/MoO₃/Ag and ITO/ZnO/Phen-NaDPO/Active Layer/Phen-NaDPO/Ag, respectively, in which Phen-NaDPO is 3-[6-(diphenylphosphinyl)-2-naphthalenyl]-1,10-phenanthroline.^[45] The hole mobilities of 5BDTBDD, 5BDDBDT and PM6 neat films are estimated to be $1.01 \times 10^{-4} \text{ cm}^2 \text{ V}^{-1} \text{ s}^{-1}$, $1.11 \times 10^{-4} \text{ cm}^2 \text{ V}^{-1} \text{ s}^{-1}$ and $1.16 \times 10^{-4} \text{ cm}^2 \text{ V}^{-1} \text{ s}^{-1}$, respectively. For blend films, the hole (μ_h) and electron (μ_e) mobilities are $2.13 \times 10^{-4} \text{ cm}^2 \text{ V}^{-1} \text{ s}^{-2}$ and $1.04 \times 10^{-4} \text{ cm}^2 \text{ V}^{-1} \text{ s}^{-2}$ of the PM6:BTP-BO4Cl binary devices. After adding 10% 5BDTBDD and 10% 5BDDBDT, the μ_h was increased to $2.38 \times 10^{-4} \text{ cm}^2 \text{ V}^{-1} \text{ s}^{-2}$ and $2.22 \times 10^{-4} \text{ cm}^2 \text{ V}^{-1} \text{ s}^{-2}$, respectively. The μ_e was increased to $1.22 \times 10^{-4} \text{ cm}^2 \text{ V}^{-1} \text{ s}^{-2}$ and $1.14 \times 10^{-4} \text{ cm}^2 \text{ V}^{-1} \text{ s}^{-2}$, respectively. Therefore, the μ_h/μ_e ratio of PM6:BTP-BO4Cl binary, PM6:5BDTBDD:BTP-BO4Cl and PM6:5BDDBDT:BTP-BO4Cl ternary devices were 2.05, 1.95 and 1.95, respectively. Here, the slight enhancement of μ_h and μ_e , when oligomer 5BDTBDD or 5BDDBDT is added, can explain the enhanced FF in optimal ternary device.

The photocurrent density (J_{ph}) versus effective voltage (V_{eff}) curves is a commonly used method for analyzing the exciton dissociation and charge collection of OSCs.^[46] Here, J_{ph} is defined as $J_L - J_D$, where J_L and J_D are current densities under illumination and in the dark, respectively. V_{eff} is determined as $V_0 - V_a$, where V_0 is the voltage when $J_{ph} = 0$, and V_a is the applied voltage. As shown in **Figure 3d**, When $V_{eff} > 2 \text{ V}$, the J_{ph} is saturated, indicating that nearly all the excitons could be dissociated into electrons and holes. Hence, exciton dissociation efficiency (η_d) or charge collection efficiency (η_c) is defined by the J_{ph}/J_{sat} values under short circuit conditions and maximum power output conditions, respectively.^[46] The η_d of PM6:5BDTBDD:BTP-BO4Cl and PM6:5BDDBDT:BTP-BO4Cl ternary OSCs (0.979 and 0.975) are slightly higher than of PM6:BTP-BO4Cl (0.972), suggesting the more efficient exciton dissociation efficiency in ternary devices. Similarly, the optimized ternary OSCs based on PM6:5BDTBDD:BTP-BO4Cl and PM6:5BDDBDT:BTP-BO4Cl exhibit a higher η_c value of 0.884 and 0.883 in comparison to the binary OSCs (0.879), indicating the more efficient charge transport and collection in ternary OSCs. These results demonstrate that introduction of oligomer as third component in the binary OSCs is an effective method to improve the η_d and η_c , and thus to improve J_{sc} and FF simultaneously.

Moreover, the charge recombination mechanism of the active layer is investigated by establishing a function between V_{OC} or J_{SC} with light intensity (P_{light}). The degree of trap-assisted recombination can be estimated by the relationship of $V_{oc} \propto nKT/q \ln(P_{light})$ (using equation edit). Here, n represents the ideality factor, K is the Boltzmann constant, T is absolute temperature, and q is the elementary charge. The slope indicates the major recombination type of OSCs. While the slope is kT/q , it suggests that bimolecular recombination is the main recombination. Once the slope is close to $2kT/q$, it indicates serious trap-assisted recombination.^[47] As shown in **Figure 3e**, the slopes of PM6:BTP-BO4Cl, PM6:5BDTBDD:BTP-BO4Cl and PM6:5BDDBDT:BTP-BO4Cl devices are 1.16 kT/q , 1.06 kT/q and 1.09 kT/q , respectively. It implies the smallest trap-assisted recombination in PM6:5BDTBDD:BTP-BO4Cl based ternary OSCs. In addition, the P_{light} dependence of J_{SC} can be described by the relation $J_{SC} \propto (P_{light})^\alpha$, which assesses the charge recombination behavior in devices. As presented in **Figure 3f**, the fitting α values in all of PM6:BTP-BO4Cl, PM6:5BDTBDD:BTP-BO4Cl and PM6:5BDDBDT:BTP-BO4Cl devices are 0.98, which is close to 1. It demonstrates the weak bimolecular recombination in both binary and ternary OSCs, which can explain the higher J_{SC} and FF of those OSCs.^[48]

Morphology Characterization

The grazing-incidence wide angle X-ray scattering (GIWAXS) characterization was applied to investigate the crystallinity and molecular orientation of the neat and blend films and the results are displayed in **Figure 4** and Figure S8. Both 5BDTBDD and 5BDDBDT neat films exhibit strong lamellar accumulation and weak π - π staking, which show a lamellar diffraction peak (100) at 0.305 \AA^{-1} and 0.324 \AA^{-1} in the out-of-plane (OOP), respectively. The crystal coherence lengths (CCLs) of 5BDTBDD and 5BDDBDT neat films are calculated as 176.63 \AA and 113.04 \AA , respectively, according the Scherrer equation: $CCLs = 2\pi K/w$, where K is the Scherrer factor ($K = 0.9$) and w is the width at the half-maximum of the peak. Besides, stronger (010) π - π stacking peak along in-plane (IP) direction and (100) lamellar diffraction in the OOP direction indicating that 5BDTBDD and 5BDDBDT neat films present dominant edge-on molecular orientation relative to the substrate. In contrast, for the BTP-BO4Cl neat film, a weak lamellar peak in the IP direction is located at 0.306 \AA^{-1} and a strong (010) π - π stacking peak appears in the OOP direction at 1.79 \AA^{-1} ($d = 3.51 \text{\AA}$, $CCLs = 25.69 \text{\AA}$), indicating that BTP-BO4Cl presents dominant face-on molecular orientation.

Interestingly, the blend film based on PM6:BTP-BO4Cl exhibits enhanced (010) diffraction peaks in the OOP direction at 1.77 \AA^{-1} ($d = 3.55 \text{ \AA}$, CCLs = 27.84 \AA). However, the (010) π - π diffraction of BTP-BO4Cl weakened when mixed with 5BDTBDD or 5BDDDBDT in binary blend films. These results indicate that the small molecular acceptor BTP-BO4Cl tends to be more miscible with 5BDTBDD and 5BDDDBDT. Compared to the blend film based on PM6:BTP-BO4Cl, the aggregation of PM6:5BDTBDD:BTP-BO4Cl and PM6:5BDDDBDT:BTP-BO4Cl-based blend films only slightly attenuated in the OOP direction, and the diffraction peaks both appear at 1.77 \AA^{-1} ($d = 3.55 \text{ \AA}$), with a CCLs of 26.91 \AA and 27.71 \AA , respectively. However, the signal strength of π - π stacking peaks of both control and ternary blend films are enhanced compared to PM6 and BTP-BO4Cl neat films. This suggests that adding structurally similar third components with higher crystallinity could finely tune the molecular packing of host molecules.

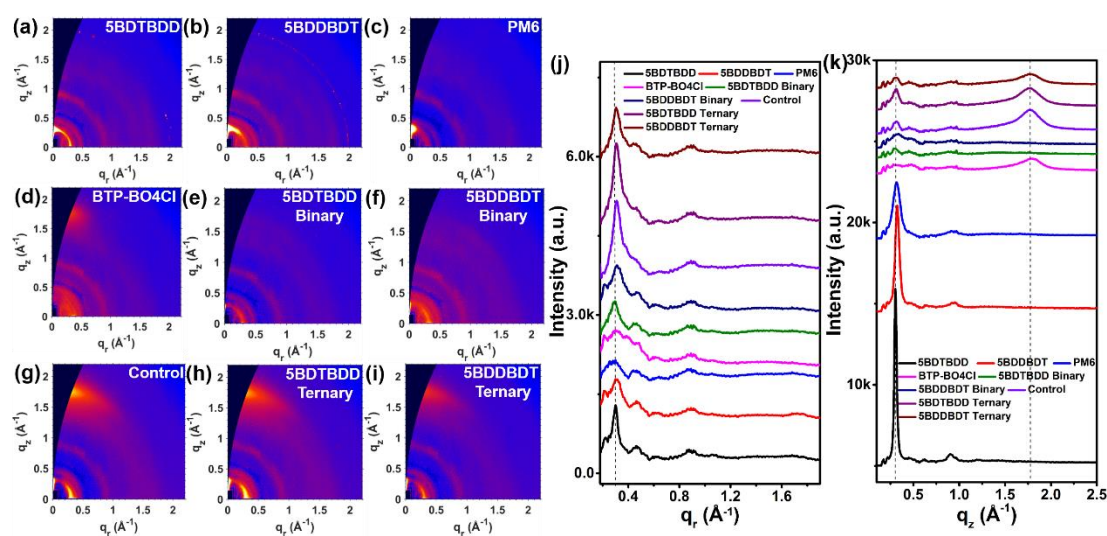


Figure 4. 2D GIWAXS patterns of a-d) neat films and e-i) blend films under optimal conditions. The 1D line cuts along j) in-plane and k) out-of-plane of the corresponding films.

To further clarify the relationship between morphological characteristics and performance, the surface morphology of the binary and ternary blends was monitored by employing atomic force microscope (AFM), as shown in **Figure 5**. The optimized ternary blend films with 10 wt% 5BDTBDD or 5BDDDBDT show weaker molecular aggregation and more uniform/smooth morphology in comparison to the control blend films. In the height images, the morphologies of the optimized PM6:BTP-BO4Cl,

PM6:5BDTBDD:BTP-BO4Cl and PM6:5BDDBDT:BTP-BO4Cl blend films exhibited root-mean-square roughness (R_q) of 1.17, 1.06, and 1.10 nm, respectively. Apparently, the binary blend film of 5BDTBDD:BTP-BO4Cl shows a smallest R_q (0.73 nm), indicating a good miscibility of the oligomer 5BDTBDD with the BTP-BO4Cl, which is consistent with the GIWAXS results. The fine-tuning morphology of ternary OSCs may be beneficial to the improvement of the exciton dissociation, charge transport and collection.^[49] Moreover, the smaller R_q roughness value of the optimized ternary blend films indicates the good compatibility of the oligomer with the hosts. It is noteworthy that the ternary blend with 50% addition value shows the similar roughness, contributing to the good composition tolerance in ternary devices with well-maintained FFs.

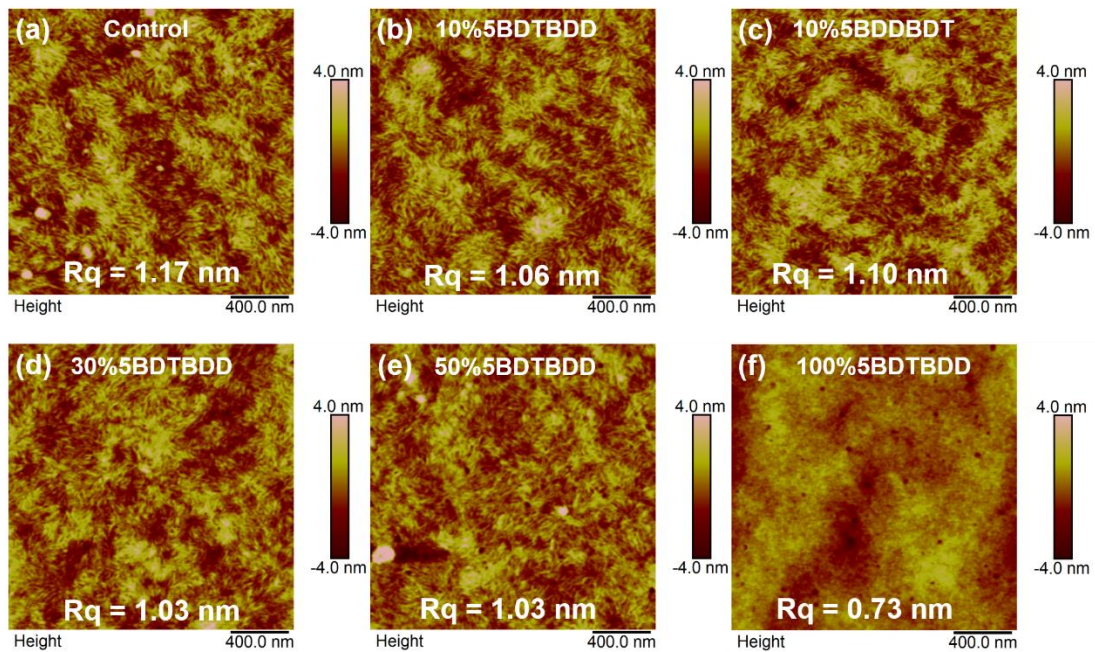


Figure 5. AFM height images for a) PM6:BTP-BO4Cl binary blend film, b) 10%5BDTBDD, c) 10%5BDDBDT, d) 30%5BDTBDD, e) 50%5BDTBDD ternary blend films, and f) 5BDTBDD:BTP-BO4Cl binary blend film.

The phase separation is an important factor affecting the performance of the device, which is affected by the compatibility between the active layer components and is fundamentally determined by the surface energy of each component. Here, two-solvent method using water and ethylene glycol (EG) was applied to determine the surface tension (γ) of the donors and acceptor and thus to estimate the tendency of intermixing

for the blend films (**Figure 6** and Table S6). As shown in **Figure 6**, the water contact angles (WCA) of the 5BDTBDD, 5BDDBDT, PM6, PM6:10%5BDTBDD, PM6:10%5BDDBDT and BTP-BO4Cl films are 98.65°, 99.77°, 104.46°, 102.41°, 102.19° and 94.10°, respectively. Besides, the EG contact angles (EgCA) of 5BDTBDD, 5BDDBDT, PM6, PM6:10%5BDTBDD, PM6:10%5BDDBDT and BTP-BO4Cl films were 74.15°, 72.91°, 71.68°, 71.34°, 70.64° and 68.31°, respectively. The corresponding surface energies were calculated to be 22.96 mN m⁻¹, 25.69 mN m⁻¹, 34.03 mN m⁻¹, 31.63 mN m⁻¹, 32.48 mN m⁻¹ and 25.81 mN m⁻¹, respectively. The contact angle results indicated that neat oligomer 5BDTBDD and 5BDDBDT films, or the blend films of PM6:10%5BDTBDD and PM6:10%5BDDBDT exhibit similar surface energy with that of BTP-BO4Cl film when compared with pure PM6 film, which implied that the mixed donor PM6:5BDTBDD and PM6:5BDDBDT films have a better compatibility with the acceptor BTP-BO4Cl, which leads to a more homogeneous and suitable phase separation morphology of the active layer. Furthermore, the equation ^[24]:

$$\gamma_{A-B} = \gamma_A + \gamma_B - 4 \left(\frac{\gamma_A^d \gamma_B^d}{\gamma_A^d + \gamma_B^d} + \frac{\gamma_A^p \gamma_B^p}{\gamma_A^p + \gamma_B^p} \right)$$

is employed to evaluate the compatibility between two different materials. Here γ_{A-B} indicates the interface tension between the material A and B, γ_A and γ_B represent the surface tension of A and B, respectively. The γ_A^d and γ_A^p are the dispersion force and the polar force, respectively, calculated by the contact angle with water and EG. Consequently, the interfacial tension of $\gamma_{5BDTBDD-BTP-BO4Cl}$ and $\gamma_{5BDDBDT-BTP-BO4Cl}$ is 0.23 and 0.71 mN m⁻¹, respectively, which is smaller than that of the $\gamma_{PM6-BTP-BO4Cl}$ (4.48 mN m⁻¹). Moreover, $\gamma_{10\%5BDTBDD-BTP-BO4Cl}$ and $\gamma_{10\%5BDDBDT-BTP-BO4Cl}$ are 3.39 and 3.70 mN m⁻¹, respectively, both are smaller than $\gamma_{PM6-BTP-BO4Cl}$. Flory–Huggins interaction parameter χ was employed to further verify the interplay among components, which are summarized in Table S6. The smaller interaction parameter between 5BDTBDD and BTP-BO4Cl ($\chi_{5BDTBDD-BTP-BO4Cl} = 0.083$) confirms that 5BDTBDD are more miscible in BTP-BO4Cl domains. These results are well consistent with the phase separation from AFM characterization. To assist visualization of morphological picture, a schematic diagram of film morphology in both binary and ternary devices was illustrated in **Figure 6c** and **6d**, respectively. These results indicate the stronger miscibility between 5BDTBDD and BTP-BO4Cl.

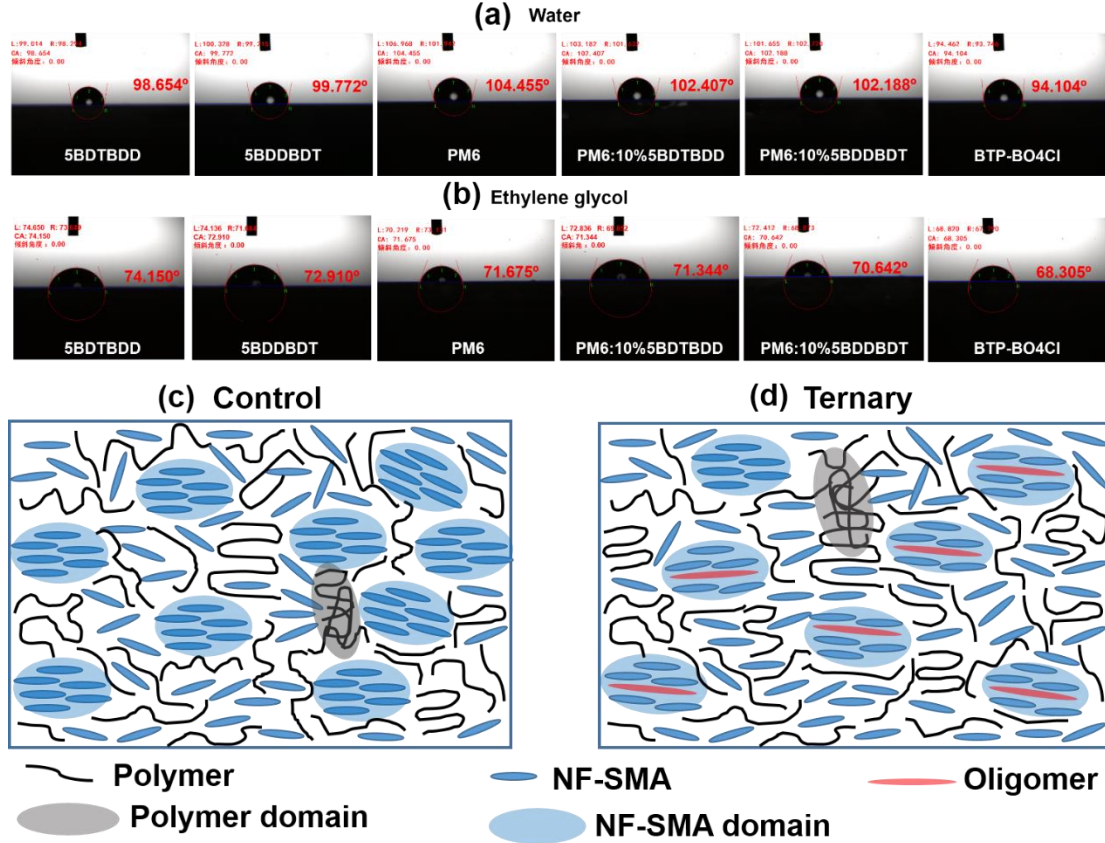


Figure 6. a-b) The contact angle images of pure films 5BDTBDD, 5BDDBDT, PM6 and BTP-BO4Cl, blend films PM6:10%5BDTBDD and PM6:10%5BDDBDT. The schematic diagrams of film morphology in c) binary devices and d) ternary devices.

Energy loss analysis

To investigate the underlying reasons behind the unusual increase of V_{oc} after incorporating the third component (5BDTBDD) with shallower HOMO energy level, we studied the detailed energy losses (E_{loss}) quantitatively in both binary and ternary devices. Following the Shockley-Queisser limit (SQ) theory, the total E_{loss} of solar cells can be divided into three terms ($\Delta E = \Delta E_1 + \Delta E_2 + \Delta E_3$)^[50,51]: 1) ΔE_1 ($E_g - qV_{oc}^{SQ}$) is the radiative recombination loss above the bandgap (E_g), which is unavoidable in any kinds of solar cells; 2) the second term, $\Delta E_2 = qV_{oc}^{SQ} - qV_{oc}^{rad}$, is assigned to the additional radiative recombination due to the disorder-induced sub-bandgap absorption, mainly coming from charge transfer state (CT) in organic solar cells.^[50] 3) ΔE_3 ($qV_{oc}^{rad} - qV_{oc}$) is non-radiative recombination loss resulting from any non-radiative recombination behaviors, such as trap-assisted recombination as well non-geminate recombination.^[51] This term is closely correlated to the external electroluminescence

quantum efficiency (EQE_{EL}), which can be calculated from the relationship of $\Delta E_3 = -kT \ln EQE_{EL}$.^[52] In the state-of-the-art non-fullerene OSCs, ΔE_2 via photogenerated CT states is considered to be less dominant in governing the V_{OC} . Efficient charge separation can be guaranteed, despite of negligible driving energy,^[14,53] in non-fullerene OSCs, while the minimal value required for efficient charge generation is believed to be 0.3 eV in fullerene OSCs.^[14] However, the PCEs of OSCs are still hindered by strong non-radiative energy loss, which is generally in the range of 0.30-0.48 eV.^[53] Thus, suppressing non-radiative recombination channels (ΔE_3) is considered to be key to further reducing the energy loss and thus maximizing the V_{OC} of OSCs.^[53] The values of E_g of both binary and ternary devices were deduced from the derivatives of the EQE_{PV} spectra edge ($dEQE/dE$),^[38] as summarized in **Table 3**. The two terms (ΔE_2 and ΔE_3) can be determined by Fourier transform photocurrent spectroscopy (FTPS) and electroluminescence (EL) techniques, respectively as shown in **Figure 7**. The detailed parameters of each loss term are summarized in **Table 3**. The binary device (PM6:BTP-BO4Cl) showed the highest photon energy loss of 0.558 eV. With the increasing content of third component (10%-50%), the E_{loss} of ternary devices decreased gradually from 0.558 eV to 0.512 eV, which is consistent with the increase of V_{OC} in the ternary solar cells. To be specific, both binary and ternary devices present similar ΔE_1 values of ~ 0.26 eV due to the almost the same E_g in the blends. The second term (ΔE_2) of all the devices is negligible (less than 0.1 eV). The ΔE_3 values of the 5BDTBDD:BTP-BO4Cl device (0.197 eV) and the ternary devices (0.207-0.230 eV) are much lower than that of the binary PM6:BTP-BO4Cl device (0.241 eV). The reduced non-radiative recombination loss is attributed to reduced overlap of the vibrational wave function of the CT states and ground states^[38] in ternary bulk-heterojunction, of which the EL spectrum exhibits blue-shift compared to that of binary device. Thus, the incorporation of 5BDTBDD has a significant contribution to the reduction of radiative and non-radiative recombination.

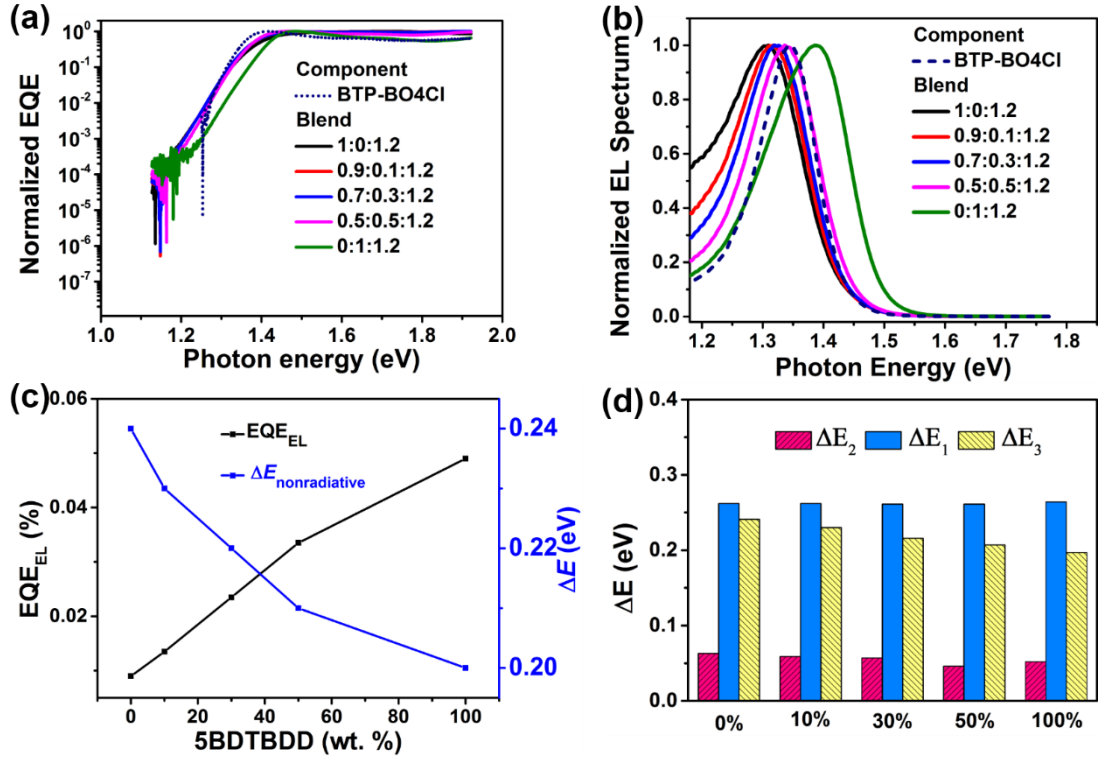


Figure 7. a) FTPS-EQEs of the binary and ternary devices with different donor components. b) Normalized EL spectra of the neat acceptor and the corresponding binary and ternary devices. c) EQE_{EL} and non-radiative recombination loss as a function of the 5BDTBDD contents. d) The comparison of ΔE_1 , ΔE_2 and ΔE_3 values of OSCs with varied 5BDTBDD contents.

Table 3. Summary of energy loss parameters of binary and ternary devices measured and calculated from FTPS-EQE and EL.

Device composition	E_g^a (eV)	V_{OC} (V)	ΔE_{loss} (eV)	$V_{OC,SQ}$ (V)	$V_{OC,rad}$ (V)	EQE _{EL} (%)	ΔE_1 (eV)	ΔE_2 (eV)	ΔE_3 (eV)	Cal. ΔE_3 (eV)
1:0:1.2	1.394	0.836	0.558	1.132	1.069	9.00E-03	0.262	0.063	0.233	0.241
0.1:0.9:1.2	1.390	0.845	0.545	1.128	1.068	1.39E-02	0.262	0.059	0.224	0.230
0.3:0.7:1.2	1.385	0.857	0.528	1.124	1.066	2.35E-02	0.261	0.057	0.210	0.216
0.5:0.5:1.2	1.385	0.873	0.512	1.124	1.077	3.35E-02	0.261	0.046	0.205	0.207
0:1:1.2	1.412	0.901	0.511	1.148	1.096	4.90E-02	0.264	0.052	0.195	0.197
Pristine acceptor	-	-	-	-	-	5.00E-02	-	-	-	-

^a E_g was obtained from the derivatives of the EQE_{PV} spectra edge. Cal. ΔE_3 is calculated with the equation $\Delta E_3 = -kT \ln EQE_{EL}$.

To further investigate the energetic disorder in the ternary devices, we plotted FTPS-EQE curves of binary and ternary devices for a comparison. As shown in **Figure 7a**, there is no significant shift of EQE edges in ternary devices compared with the PM6:BTP-BO4Cl device (1:0:1.2). Noticeably, the EQE edges of ternary devices became sharper in the low-energy region which can explain minimal radiative recombination loss below the bandgap (ΔE_2). As depicted in Figure S9, the optimized ternary device (0.9:0.1:1.2) showed a smaller Urbach energy (E_U) of 23.9 meV than

that of binary counterparts (26.4 meV). When further increasing 5BDTBDD contents, E_U gradually decreased from 23.8 to 22.8 meV in ternary devices, indicating reduce energetic disorder in ternary blends. Compared to the control blend (1:0:1.2), the measured EL peaks of the ternary blends displayed obviously blue-shifted trend as the content of 5BDTBDD increased, which is approaching that of pristine acceptor BTP-BO4Cl, indicating an increasing energy of charge transfer state (E_{CT}) in ternary bulk-heterojunction. We speculate that the strong crystallinity of 5BDTBDD could modulate the E_{CT} and thus reduce the non-radiative recombination rate.^[54] Interestingly, the EL peak of pristine BTP-BO4Cl was located at around 1.345 eV, while the EL peak of 5BDTBDD:BTP-BO4C blend was found to be shifted to high-energy area of 1.345 eV, which is abnormal in the OSCs research that may be related to the molecular packing of acceptor. We assume that the aggregation-caused emission quenching effect (ACQ) of acceptor can be sharply reduced. It has been reported that in the case of low driving energy based OSCs, the emission of the device preferably originates from the pristine materials with the lowest bandgaps rather than CT state.^[54] To further access the non-radiative energy loss of devices, we measured EQE_{EL} of the devices, as illustrated in **Figure 7c** and detailed values are summarized in **Table 3**. We found that the EL efficiencies of all the ternary blends are high at 10^{-4} , one order of magnitude higher than that of the control blend (9×10^{-5}). Consequently, the ΔE_3 values of control device (1:0:1.2) and ternary devices (0.9:0.1:1.2, 0.3:0.7:1.2, 0.5:0.5:1.2) were calculated to be 0.241, 0.230, 0.216 and 0.207 eV, respectively, displaying a monotonically declining trend with more loading of 5BDTBDD. These calculated ΔE_3 values are well consistent to the those calculated via the $qV_{\text{oc}}^{\text{rad}} - qV_{\text{oc}}$ equation. It was worth mentioning that ΔE_2 of ~ 0.20 eV is among the lowest in the high-performance OSCs systems. More importantly, the external EL quantum efficiency of 5BDTBDD:BTP-BO4Cl (4.9×10^{-4}) is as high as that of pristine acceptor (5×10^{-4}), as shown in **Table 3**. The comparable emission efficiency after blending 5BDTBDD support our assumption that the ACQ effect of BTP-BO4Cl can be significantly reduced due to the excellent miscibility between 5BDTBDD and BTP-BO4Cl, and consequently, the EQE_{EL} can be enhanced by about one order of magnitude.^[55] Overall, we attribute the

abnormal enhancement of V_{OC} after addition of third component with higher HOMO energy level to the significantly inhibited ΔE_2 and ΔE_3 (as visually shown in **Figure 7d**).

4. Conclusion

In summary, we developed high-performance ternary OSCs using two submolecules (oligomers) of classic polymer donor PBDB-T, named 5BDTBDD and 5BDDBDT with D-A-D-A-D and A-D-A-D-A backbone configuration as the third components, respectively. Better comparability between oligomers and BTP-BO4Cl was favorable to the fine-tuning of active layer morphology and thus to the promotion of FF and J_{SC} in ternary OSCs. Importantly, the detailed energy loss analysis demonstrated an abnormal V_{OC} enhancement mechanism in optimal ternary devices, in which non-radiative recombination suppression overweighs the third component HOMO level influence. The new results provide a novel V_{OC} loss mechanism understanding in ternary OSCs. As a result, the ternary OSCs based on PM6:5BDTBDD:BTP-BO4Cl and PM6:5BDDBDT:BTP-BO4Cl achieved an outstanding PCE of 17.54% and 17.32%, processed by green solvent *o*-xylene. Moreover, the strategy with novel oligomers as the third components also exhibits an excellent composition tolerance in ternary OSCs. Overall, our work demonstrates that structurally compatible oligomers are effective third components to synergistically reduce energy loss and optimize morphology towards high-performance OSCs.

Acknowledgement

H. X. and Y. Z. contributed equally to this work. This work was supported by the National Natural Science Foundation of China (51673031, 51573154, 51573107, 91633301 and 21432005), the Major Program of the Natural Science Research of Jiangsu Higher Education Institutions (18KJA480001), the Top-notch Academic Programs Project of Jiangsu Higher Education Institutions (TAPP), A Project Funded by the Priority Academic Program Development of Jiangsu Higher Education Institutions (PAPD), Jiangsu Provincial Talents Project of High-Level Innovation and Entrepreneurship, the Research Innovation Program for Postgraduate of Jiangsu Province (KYCX19_1751), the Research Grants Council of Hong Kong (GRF grant 15218517, CRF C5037-18G, PDFS2021-5S04), National Science Foundation of China (NSFC51961165102), the Shenzhen Science and Technology Innovation Commission

(JCYJ 20200109105003940), the Sir Sze-yuen Chung Endowed Professorship Fund (8-8480) and RISE fund (CDA5) provided by the Hong Kong Polytechnic University. The authors especially thank National Synchrotron Radiation Research Center (Taiwan) for the support in the GIWAXS characterization.

Supporting Information

Details of characterization, measurement and synthetic methods; ^1H , ^{13}C NMR spectra and Time-of-Flight (MALDI-TOF) analyzer data; TGA, DSC, UV, DFT, *J-V*, PL, SCLC, GIWAXS, Contact Angle and Energy Loss measurement data.

References

- [1] G. Yu, J. Gao, J. C. Hummelen, F. Wudi, A. J. Heeger, *Science* **1995**, *270*, 1789.
- [2] Y. Cheng, S. Yang, C. Hsu, *Chem. Rev.* **2009**, *109*, 5868.
- [3] G. Li, R. Zhu, Y. Yang, *Nat. Photon.* **2012**, *6*, 153.
- [4] L. Dou, Y. Liu, Z. Hong, G. Li, Y. Yang, *Chem. Rev.* **2015**, *115*, 12633.
- [5] S. Li, C.-Z. Li, M. Shi, H. Chen, *ACS Energy Lett.* **2020**, *5*, 1554.
- [6] Q. Liu, Y. Jiang, K. Jin, J. Qin, J. Xu, W. Li, J. Xiong, J. Liu, Z. Xiao, K. Sun, S. Yang, X. Zhang, L. Ding, *Sci. Bull.* **2020**, *65*, 272.
- [7] Y. Lin, Y. Firdaus, F. H. Isikgor, M. I. Nugraha, E. Yengel, G. T. Harrison, R. Hallani, A. El-Labban, H. Faber, C. Ma, X. Zheng, A. Subbiah, C. T. Howells, O. M. Bakr, I. McCulloch, S. D. Wolf, L. Tsetseris, T. D. Anthopoulos, *ACS Energy Lett.* **2020**, *5*, 2935.
- [8] Y. Lin, M. I. Nugraha, Y. Firdaus, A. D. Scaccabarozzi, F. Aniés, A.-H. Emwas, E. Yengel, X. Zheng, J. Liu, W. Wahyudi, E. Yarali, H. Faber, O. M. Bakr, L. Tsetseris, M. Heeney, T. D. Anthopoulos, *ACS Energy Lett.* **2020**, *5*, 3663.
- [9] C. Li, J. Zhou, J. Song, J. Xu, H. Zhang, X. Zhang, J. Guo, L. Zhu, D. Wei, G. Han, J. Min, Y. Zhang, Z. Xie, Y. Yi, H. Yan, F. Gao, F. Liu, Y. Sun, *Nat. Energy* **2021**, *6*, 605.

- [10] F. Liu, L. Zhou, W. Liu, Z. Zhou, Q. Yue, W. Zheng, R. Sun, W. Liu, S. Xu, H. Fan, L. Feng, Y. Yi, W. Zhang, X. Zhu, *Adv. Mater.* **2021**, *33*, 2100830.
- [11] Y. Zhang, K. Liu, J. Huang, X. Xia, J. Cao, G. Zhao, P.W.K. Fong, Y. Zhu, F. Yan, Y. Yang, X. Lu, G. Li, *Nat. Com.* **2021**, *12*, 4815.
- [12] J.D. Zimmerman, X. Xiao, C.K. Renshaw, S. Wang, V.V. Diev, M.E. Thompson, S.R. Forrest, *Nano Lett.* **2012**, *12*, 4366.
- [13] Y. Chang, J. Zhang, Y. Chen, G. Chai, X. Xu, L. Yu, R. Ma, H. Yu, T. Liu, P. Liu, Q. Peng, H. Yan, *Adv. Energy Mater.* **2021**, *11*, 2100079.
- [14] J. Liu, S. Chen, D. Qian, B. Gautam, G. Yang, J. Zhao, J. Bergqvist, F. Zhang, W. Ma, H. Ade, O. Inganäs, K. Gundogdu, F. Gao, H. Yan, *Nat. Energy* **2016**, *1*, 1.
- [15] N. An, Y. Cai, H. Wu, A. Tang, K. Zhang, X. Hao, Z. Ma, Q. Guo, H. S. Ryu, H. Y. Woo, Y. Sun, E. Zhou, *Adv. Mater.* **2020**, *32*, 2002122.
- [16] Y. Zhang, D. Liu, T. K. Lau, L. Zhan, D. Shen, P. W. K. Fong, C. Yan, S. Zhang, X. Lu, C. S. Lee, J. Hou, H. Chen, G. Li, *Adv. Funct. Mater.* **2020**, *30*, 1910466.
- [17] Q. An, J. Wang, X. Ma, J. Gao, Z. Hu, B. Liu, H. Sun, X. Guo, X. Zhang, F. Zhang, *Energy Environ. Sci.* **2020**, *13*, 5039.
- [18] L. Zhan, S. Li, T.-K. Lau, Y. Cui, X. Lu, M. Shi, C.-Z. Li, H. Li, J. Hou, H. Chen, *Energy Environ. Sci.* **2020**, *13*, 635.
- [19] X. Ma, J. Wang, J. Gao, Z. Hu, C. Xu, X. Zhang, F. Zhang, *Adv. Energy Mater.* **2020**, *10*, 2001404.
- [20] R. Ma, T. Liu, Z. Luo, K. Gao, K. Chen, G. Zhang, W. Gao, Y. Xiao, T.-K. Lau, Q. Fan, Y. Chen, L.-K. Ma, H. Sun, G. Cai, T. Yang, X. Lu, E. Wang, C. Yang, A. K. Y. Jen, H. Yan, *ACS Energy Lett.* **2020**, *5*, 2711.
- [21] X. Xu, Y. Li, Q. Peng, *Nano Select* **2020**, *1*, 30.
- [22] Q. An, F. Zhang, J. Zhang, W. Tang, Z. Deng, B. Hu, *Energy Environ. Sci.*, **2016**, *9*, 281.
- [23] B. Fan, W. Zhong, X. Jiang, Q. Yin, L. Ying, F. Huang, Y. Cao, *Adv. Energy Mater.* **2017**, *7*, 1602127.

- [24] R. Yu, H. Yao, Y. Cui, L. Hong, C. He, J. Hou, *Adv. Mater.* **2019**, *31*, 1902302.
- [25] Z. Wang, X. Zhu, J. Zhang, K. Lu, J. Fang, Y. Zhang, Z. Wang, L. Zhu, W. Ma, Z. Shuai, Z. Wei, *J. Am. Chem. Soc.* **2018**, *140*, 1549.
- [26] Y. Yang, W. Chen, L. Dou, W. Chang, H. Duan, B. Bob, G. Li, Y. Yang, *Nat. Photon* **2015**, *9*, 190.
- [27] R. Yu, S. Zhang, H. Yao, B. Guo, S. Li, H. Zhang, M. Zhang, J. Hou, *Adv. Mater.* **2017**, *29*, 1700437.
- [28] L. Zhong, L. Gao, H. Bin, Q. Hu, Z.-G. Zhang, F. Liu, T. P. Russell, Z. Zhang, Y. Li, *Adv. Energy Mater.* **2017**, *7*, 1602215.
- [29] W. Li, D. Wang, S. Wang, W. Ma, S. Hedstrom, D. I. James, X. Xu, P. Persson, S. Fabiano, M. Berggren, O. Inganas, F. Huang, E. Wang, *ACS Appl. Mater. Interfaces* **2015**, *7*, 27106.
- [30] L. Yuan, K. Lu, B. Xia, J. Zhang, Z. Wang, Z. Wang, D. Deng, J. Fang, L. Zhu, Z. Wei, *Adv. Mater.* **2016**, *28*, 5980.
- [31] J. Wang, K. K. Liu, J. Yan, Z. Wu, F. Liu, F. Xiao, Z. F. Chang, H. B. Wu, Y. Cao, T. P. Russell, *J. Am. Chem. Soc.* **2016**, *138*, 7687.
- [32] L. Yuan, Y. Zhao, J. Zhang, Y. Zhang, L. Zhu, K. Lu, W. Yan, Z. Wei, *Adv. Mater.* **2015**, *27*, 4229.
- [33] H. Xia, X. Xu, J. Guo, C. Qian, K. Zhang, M. Zhu, B. Zhang, W. Peng, Q. Peng, W. Zhu, *Dyes and Pigments* **2021**, *186*, 108950.
- [34] W. Peng, G. Zhang, L. Shao, C. Ma, B. Zhang, W. Chi, Q. Peng, W. Zhu, *J. Mater. Chem. A* **2018**, *6*, 24267.
- [35] M. Li, Z. Qiu, G. Zhang, Y. Liu, L. Xiong, D. Bai, M. Zhu, Q. Peng, W. Zhu, *J. Mater. Chem. A* **2018**, *6*, 12493.
- [36] P. Bi, X. Hao, *Solar RRL* **2019**, *3*, 1800263.
- [37] Y. Zhang, G. Li, *Acc. Mater. Res.* **2020**, *1*, 158.
- [38] Y. Wang, D. Qian, Y. Cui, H. Zhang, J. Hou, K. Vandewal, T. Kirchartz, F. Gao, *Adv. Energy Mater.* **2018**, *8*, 1801352.

- [39] C. Yang, J. Zhang, N. Liang, H. Yao, Z. Wei, C. He, X. Yuan, J. Hou, *J. Mater. Chem. A* **2019**, *7*, 18889.
- [40] M. J. Frisch, G. W. Trucks, H. B. Schlegel, G. E. Scuseria, M. A. Robb, J. R. Cheeseman, V. G. Zakrzewski, J. A. Montgomery, R. E. Stratmann, J. C. Burant, S. Dapprich, J. M. Millam, A. D. Daniels, K. N. Kudin, M. C. Strain, O. Farkas, J. Tomasi, V. Barone, M. Cossi, R. Cammi, B. Mennucci, C. Pomelli, C. Adamo, S. Clifford, J. Ochterski, G. A. Petersson, P. Y. Ayala, Q. Cui, K. Morokuma, D. K. Malick, A. D. Rabuck, K. Raghavachari, J. B. Foresman, J. Cioslowski, J. V. Ortiz, A. G. Baboul, B. B. Stefanov, G. Liu, A. Liashenko, P. Piskorz, I. Komaromi, R. Gomperts, R. L. Martin, D. J. Fox, T. Keith, M. A. Al-Laham, C. Y. Peng, A. Nanayakkara, M. Challacombe, P. M. W. Gill, B. G. Johnson, W. Chen, M. W. Wong, J. L. Andres, C. Gonzalez, M. HeadGordon, E. S. Replogle, J. A. Pople, Gaussian98; Gaussian, Inc.: Pittsburgh, PA, 2001.
- [41] H. Yao, Y. Cui, D. Qian, C. S. Ponseca, A. Honarfar, Y. Xu, J. Xin, Z. Chen, L. Hong, B. Gao, R. Yu, Y. Zu, W. Ma, P. Chabera, T. Pullerits, A. Yartsev, F. Gao, J. Hou, *J. Am. Chem. Soc.* **2019**, *141*, 7743.
- [42] Y. Cui, H. Yao, L. Hong, T. Zhang, Y. Tang, B. Lin, K. Xian, B. Gao, C. An, P. Bi, W. Ma, J. Hou, *Natl. Sci. Rev.* **2020**, *7*, 1239.
- [43] Y. Chen, R. Ma, T. Liu, Y. Xiao, H. K. Kim, J. Zhang, C. Ma, H. Sun, F. Bai, X. Guo, K. S. Wong, X. Lu, H. Yan, *Adv. Energy Mater.* **2021**, *11*, 2003777.
- [44] W. Su, Q. Fan, X. Guo, X. Meng, Z. Bi, W. Ma, M. Zhang, Y. Li, *Nano Energy* **2017**, *38*, 510.
- [45] W.-Y. Tan, R. Wang, M. Li, G. Liu, P. Chen, X.-C. Li, S.-M. Lu, H. L. Zhu, Q.-M. Peng, X.-H. Zhu, W. Chen, W. C. H. Choy, F. Li, J. Peng, Y. Cao, *Adv. Funct. Mater.* **2014**, *24*, 6540.
- [46] P. W. M. Blom, V. D. Mihailetschi, L. J. A. Koster, D. E. Markov, *Adv. Mater.* **2007**, *19*, 1551.
- [47] L. J. A. Koster, V. D. Mihailetschi, R. Ramaker, P. W. M. Blom, *Appl. Phys. Lett.* **2005**, *86*, 123509.

- [48] L. Nian, K. Gao, Y. Jiang, Q. Rong, X. Hu, D. Yuan, F. Liu, X. Peng, T. P. Russell, G. Zhou, *Adv. Mater.* **2017**, *29*, 1700616.
- [49] J. Cai, X. Zhang, C. Guo, Y. Zhuang, L. Wang, D. Li, D. Liu, T. Wang, *Adv. Funct. Mater.* **2021**, *31*, 2102189.
- [50] J. Yao, T. Kirchartz, M. S. Vezie, M. A. Faist, W. Gong, Z. He, H. Wu, J. Troughton, T. Watson, D. Bryant, J. Nelson, *Phys. Rev. Appl.* **2015**, *4*, 014020.
- [51] W. Shockley, H. J. Queisser, *J. Appl. Phys.* **1961**, *32*, 510.
- [52] U. Rau, *Phys. Rev. B* **2007**, *76*, 085303.
- [53] D. Qian, Z. Zheng, H. Yao, W. Tress, T. R. Hopper, S. Chen, S. Li, J. Liu, S. Chen, J. Zhang, X.-K. Liu, B. Gao, L. Ouyang, Y. Jin, G. Pozina, I. A. Buyanova, W. M. Chen, O. Inganäs, V. Coropceanu, J.-L. Bredas, H. Yan, J. Hou, F. Zhang, A. A. Bakulin, F. Gao, *Nat. Mater.* **2018**, *17*, 703.
- [54] J. Hou, O. Inganäs, R. H. Friend, F. Gao, *Nat. Mater.* **2018**, *17*, 119.
- [55] Y. Qin, S. Zhang, Y. Xu, L. Ye, Y. Wu, J. Kong, B. Xu, H. Yao, H. Ade, J. Hou, *Adv. Energy Mater.* **2019**, *9*, 1901823.